Dynamic Inhomogeneities in Polymer Gels Investigated by Dynamic Light Scattering

Tomohisa Norisuye* and Qui Tran-Cong-Miyata

Department of Polymer Science and Engineering, Kyoto Institute of Technology, Matsugasaki, Sakyo-ku, Kyoto 606-8585, Japan

Mitsuhiro Shibayama

Neutron Science Laboratory, Institute for Solid State Physics, 106-1 Shirakata, The University of Tokyo, Tokai, Naka-gun, Ibaraki 319-1106, Japan

Received August 22, 2003; Revised Manuscript Received February 1, 2004

ABSTRACT: Position-dependent dynamic fluctuations in polymer gels have been investigated by dynamic light scattering (DLS). DLS measurements were performed over a hundred sampling points by rotating test tubes for as-prepared and swollen gels in order to probe different scattering volumes. The time-averaged scattered intensities obtained by DLS were decomposed into two contributions, i.e., thermal fluctuations, I_F, and time-independent frozen inhomogeneities, I_C. The two variables were analyzed as a function of sampling position, where not only I_C but also I_F were considered to be position dependent. As often observed in gelling systems, I_C generally dominates in comparison with I_F irrespective of the method of cross-linking. Here, we propose a nonergodic method to examine whether position dependent fluctuations in $I_F(p)$ observed experimentally are due to the nature of gels or to an experimental noise. For gels with high cross-linking densities, dynamic inhomogeneities are observed as a result of the difference in the molecular environment, e.g., the difference in the local gel concentration and/or cross-linking density, resulting in the emergence of position dependence of I_F as well as that of the homodyne diffusion coefficient, D. We will also address the importance of a third component, i.e., the low molecular weight species, I_S, in the analysis of the dynamics of polymer gels.

Introduction

Polymer gels are produced by polymerization of monomers in the presence of multifunctional cross-linkers or introduction of intermolecular cross-links into polymer solutions. In some respects, gels resemble the corresponding polymer solutions, while cross-links provide unique properties such as moderate rigidity, capability of shape retention and gradual release of small molecules.[1,2] Due to topological constrains by cross-links the segmental motion of the network chains is highly restricted, leading to an emergence of time-independent quenched-concentration fluctuations called frozen inhomogeneities.[3,4] Studies on frozen inhomogeneities become crucial in order to elucidate the nature of gels. An upturn in X-ray or neutron scattered intensities at low angles compared to the corresponding solutions[5−7] and position-dependent strong fluctuations in light scattered intensities called "speckles"[8−12] are typical examples of the signature of frozen inhomogeneities. Until the discovery of frozen inhomogeneities, the scattered intensity of gels was considered to be lower than that of the corresponding polymer solutions due to the existence of the elastic modulus since it significantly suppresses the concentration fluctuations. However, it was found that reduction of scattered intensity in a gel appears in dynamic part, whereas the total intensities become much larger than those of the polymer solutions due to the inhomogeneities. Pusey and van Megen first formulated the equations for dynamic light scattering theory for nonergodic medium.[13,14] They derived time- and ensemble-average time−intensity correlation functions of gels by introducing fluctuating and the time-independent concentration fluctuations, corresponding respectively to the dynamic fluctuations, I_F, and the frozen inhomogeneities, I_C.

Until the present, the following results are evident by a great number of studies: (1) I_C is much larger than I_F and increases further by swelling.[3,15−17] An increase of I_C by uniaxial elongation of gels appears in the stretched direction rather than in the perpendicular direction (butterfly pattern).[18−21] Moreover, an anomalous two-dimensional scattering profile, i.e., abnormal butterfly pattern, was also observed for polyelectrolyte gels[22] and was explained by the theory.[23] (2) I_C exhibits strong fluctuations with the sampling position but I_F does not. As a matter of fact, the intensity distribution function is often exhibited by a Poisson distribution of I_C with a sharp lower cutoff at I_F.[8,15] (3) I_C increases with the cross-linking density[8,24] and the interaction parameter at preparation.[25,26] This is why I_C is called quenched or frozen inhomogeneities. In other words, gels memorize the initial state how they are prepared. I_C also depends on the observation temperature and the way of cross-linking.[27,28] (4) I_F strongly depends on the observation temperature,[29] whereas it is almost independent of the preparation temperature. [25,26,30] It was due to the fact that I_F is a dynamic quantity and is free from the frozen inhomogeneities. I_F is also a weak function of the cross-linking density. (5) Since the appearance of I_C is characteristic in a gelling system, it can be applied to the determination of gel point.[31] In our previous works, we developed a time-resolved dynamic light scattering method to elucidate the kinetics and the mechanism of the gelation[32,33] and/or aggregation.[34]

Contrary to the frozen inhomogeneities, position-dependent dynamic fluctuations have not been well investigated. This may be ascribed to the fact that the

* To whom correspondence should be addressed.

10.1021/ma035246d CCC: $27.50
Published on Web 03/16/2004

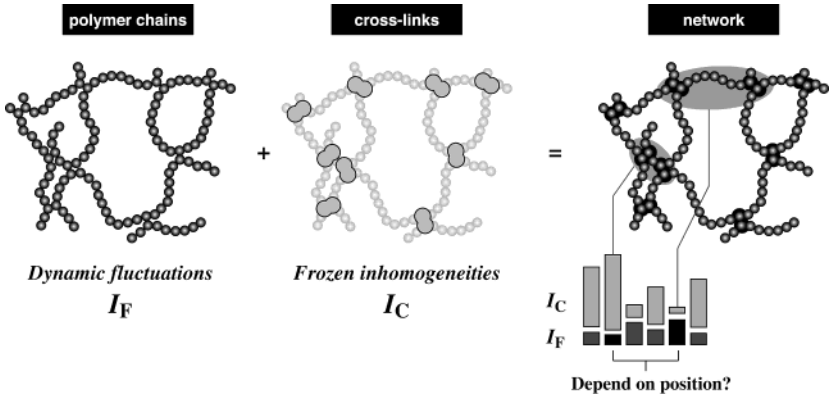

Figure 1. Schematic representation of the network structure consisting of polymer chains and cross-links. The physical interpretation of the intensity components for the dynamic and frozen inhomogeneities is also given.

dynamic part of the concentration fluctuations is considered to be equivalent to that for the corresponding solutions, resulting in a position-independent character. However, the elastic contribution of the free energy was not taken into account in this interpretation. Hence, it is envisaged that the dynamic fluctuations for gels are not equal to that for solutions without cross-links.[6,27,35] Furthermore, I_F may be more or less dependent on molecular environment, such as local gel concentration and/or cross-linking density, since the displacement of the chain segments is highly restricted by cross-links with different degrees. Schematic representations of the frozen inhomogeneities and the dynamic fluctuations are given in Figure 1. For the higher cross-linking density region, the contribution from the frozen inhomogeneities becomes larger whereas the dynamic part may be smaller. Thus, the time average dynamic fluctuations may be confined in the limited region, resulting in position dependent character. More recently, Furukawa and Hirotsu proposed an alternative method to treat the static and dynamic inhomogeneities of gels.[36] They derived the ensemble averaged field correlation function, $g_E^{(1)}(\tau)$, by considering the "spatial coupling" of the scattering field components for fluctuating, $E_F(t)$, and time-independent components, E_C. As a result, they predicted a nonzero baseline of the ensemble averaged correlation function, $g_E^{(1)}(\infty)$. This is equivalent to the contribution of the frozen inhomogeneities to the total intensity for various kinds of gels including the case where E_F and E_C are not spatially independent. They argued that the general Siegert equation[37] produces a serious underestimation of $g_E^{(1)}(\infty)$ in comparison with their result given by[36]

$$g_E^{(2)}(\tau) = 1 + |g_E^{(1)}(\tau)|^2 + 2\delta_E(\tau) \quad (1)$$

Here $\delta_E(\tau)$ represents an extra term due to the coupling between E_F and E_C. On the other hand, such kind of coupling is not significant for the time average but for the spatial average. Hence

$$\langle E_F E_C^* \rangle_P \neq \langle E_F \rangle_P \langle E_C^* \rangle_P \quad (2)$$

$$\langle E_F E_C^* \rangle_T = \langle E_F \rangle_T E_C^* \quad (3)$$

Here $\langle ... \rangle_P$ and $\langle ... \rangle_T$, respectively, denote spatial and time average and the asterisk indicates the complex conjugate. Indeed, they derived eq 1 by considering eqs 2 and 3. We will discuss dynamic inhomogeneities in terms of the time-averaged equations as a function of sampling position without ensemble averaging. In this case, it is not necessary whether the spatial correlation between E_F and E_C exists or not. Nevertheless, it is still cumbersome and difficult to judge whether position-dependent fluctuations are a signature of the dynamic inhomogeneities or not. Therefore, we demonstrate a different approach to evaluate the position-dependent intensity components, I_F and I_C, by deeply taking into account the partial heterodyne nature of gels.

Experimental Section

Samples. Preparation of γ-ray Gels. In our previous studies, two types of poly(*N*-isopropylacrylamide)(PNIPA) gels were prepared by redox polymerization(monomer cross-linked gels) and by γ-ray irradiation(polymer cross-linked gels) for comparison of the network structures.[27,28] Cross-links are introduced randomly in space for the polymer cross-linked gels, whereas the distribution of cross-linking points for the monomer cross-linked gels is more inhomogeneous due to difference in the reactivity ratios of monomers and cross-linkers.[38−40] In this study, the two types of gels are employed in order to investigate the effect of cross-linking and the distribution.

NIPA monomer powder, supplied by Kohjin Chemical Co., was purified by dissolving in toluene and recrystallizing in petroleum ether prior to use. Reagent grade APS was purchased from Wakenyaku Co. Ltd. and was used without further purification. PNIPA aqueous solutions were prepared by redox polymerization of NIPA monomer at 20°C in the presence of *N*,*N*,*N*′,*N*′-tetramethylethylenediamine (TEMED; accelerator) and ammonium persulfate (APS; initiator) in advance to γ-ray irradiation. The monomer solutions were filtered through a 0.2 μm pore size filter before initiating the reaction. Irradiation of γ-rays was carried out by a ^{60}Co source, where the sample was regulated with a thermostat bath at preparation temperatures such as 0, 20, 27, and 30 °C. The γ-ray gels having different cross-linking densities were obtained with different irradiation times ranging from 0.5 to 8.0 h at constant dose rate of about 10 kGy/h. All the samples were transparent even for the highest irradiation dose.

Preparation of Washed Gels. The above obtained γ-ray gels were used without any purification/equilibration in the experiments. It allows us to perform DLS measurements without uncertainty due to (1) accidental scattering at the interference between the gel and the test tube and (2) unexpected baseline elevation in the correlation function due to slow moving of the entire gel. That is why we have been employing as-prepared gels in the DLS studies. On the other hand, as-prepared gels contain unreacted monomers, sol fraction, and some residues. Therefore, washed gels were also prepared by quickly elevating the temperature to 50 °C, followed by an addition of equal amount of solvents and aging at 20 °C more than a week. Note that the gels are put back into another test tube having the same diameter at preparation. Therefore, the swelling degree was the same as that of the as-prepared gel. The effects of remaining impurities and

some rearrangement of the network structure may become evident by this experiment.

Preparation of Fully Swollen Electrolyte Gels. To investigate the effect of swelling on the dynamic inhomogeneities, poly(*N*-isopropylacrylamide-*co*-sodium acrylate) gels, PNIPA-SA gels, were prepared. First 658 mM of NIPA monomer, 32 mM of sodium acrylate (SA), 8.62 mM of *N*,*N*′-methylenebisacrylamide (BIS; cross-linker), and 1.75 mM of APS were dissolved in distilled water and degassed. After the solution was chilled in a refrigerator, 8 mM of TEMED was added in order to initiate redox copolymerization as well as cross-linking. The polymerization was conducted at 20 °C for 24 h. Samples for DLS measurements were made in a test tube with inner diameter of 4 mm, which was small enough for spontaneous swelling in a larger test tube at a given pH. The gels thus prepared were taken out from the mold and washed in distilled water and then transferred to another test tube with 8 mm diameter.

Dynamic Light Scattering. Dynamic light scattering (DLS) measurements were carried out with a DLS/SLS-5000 compact goniometer, ALV, Langen, coupled with an ALV photon correlator. A 22 mW helium−neon laser was used as the incident beam with the wavelength, $\lambda = 632.8$ nm. In our present geometry of DLS, a high counting rate of the scattered intensity and a high coherence in ICF were achieved owing to employment of a set of a static/dynamic enhancers and a high-quantum efficient avalanche−photodiode detection system with an optical fiber. The apparatus constant, β, related to the number of coherence, n, with $\beta \sim n^{-1/2}$, is found to be 0.988 according to the analysis of the standard LATEX dilute solutions. Since the intensity and the electric field correlation functions are linked by

$$g_T^{(2)}(\tau) = 1 + \beta|g_T^{(1)}(\tau)|^2 \tag{4}$$

one can evaluate β from the initial amplitude of the intensity correlation function. Here $g_T^{(2)}(\tau)$ and $g_T^{(1)}(\tau)$ are, respectively, the time-averaged intensity and the electric field correlation functions. In general, the number of coherence areas can be varied by adjusting the size of two pinholes. In our system, further enhancement of the coherence compared to the conventional DLS system was achieved by the fiber detection rather than two variable pinholes, resulting in an almost single coherent area being probed. All the ICF data have been corrected by $\beta = 0.99$ to ensure the discussion of the solvent effect in the present paper.

Time-averaged intensity and the corresponding intensity−correlation function (ICF) were obtained with an acquisition time of 30 s for each run. The intensities and ICFs were collected with various scattering positions by rotating the test tube at fixed scattering angle of 90°. The temperature was regulated by a thermostated bath within ±0.1°C.

To protect the detector from strong incident beam, we reduced the incident beam intensity with a neutral density filter, which is particularly important for an avalanche−photodiode detection system. A series of sample rotation measurements was performed by keeping the scattered intensity being lower than 200 kHz. In this way, the problem due to detector dead time and the correlator saturation can be circumvented. Thus, the obtained intensities were corrected depending on the level of the incident beam. In addition, the efficiency of the density filter was also checked by a fluorescence probe, e.g., methylene blue (MB).

Simulation. Simple simulations for I_F and I_C with a certain correlation between them were carried out in order to demonstrate the intensity variations with different conditions. Position-dependent intensities, $I_F(p)$ and $I_C(p)$, were produced with a computer generated zero-mean Gaussian noise, $w(p)$ according to the following equations.

$$I_F(p) = \langle I_F \rangle_p + A_F w(p) \tag{5}$$

$$I_C(p) = \begin{cases} C \exp[Z(0)A_C w(p)] & \text{for } Z = \pm 1 \\ C \exp[A_C w'(p)] & \text{for } Z = 0 \end{cases} \tag{6}$$

Here, $w'(p)$ is another set of noise if there is no correlation between $I_F(p)$ and $I_C(p)$. C is a constant, A_F and A_C, respectively, are the magnitudes of the dynamic and static inhomogeneities. Z is the cross-correlation function of $I_F(p)$ and $I_C(p)$ given by

$$Z(\Delta p) = \frac{\langle (I_C(p) - \langle I_C \rangle_p)(I_F(p + \Delta p) - \langle I_F \rangle_p) \rangle_p}{\sqrt{\langle (I_C - \langle I_C \rangle_p)^2 \rangle_p} \sqrt{\langle (I_F - \langle I_F \rangle_p)^2 \rangle_p}} \tag{7}$$

where $Z(0)$ equals -1 if $I_F(p)$ monotonically decreases with $I_C(p)$ (negative correlation) and $+1$ if $I_F(p)$ increases with $I_C(p)$ (positive correlation). Note that for the static component, the intensity distribution often exhibited negative exponential with lower cutoff rather than the Gauss distribution. To achieve more realistic intensity variations for the static components, the exponential function, eq 6, was employed. Thus, a data set of $I_F(p)$ and $I_C(p)$ with various correlations can be easily compared. Here, a larger number of the data points would make better results, but a hundred points are enough to confirm the behavior of $I_F(p)$ against the total intensity. In addition, the effect of a third component, I_S, due to solvents, sol fraction, and residues are taken into account. A theoretical consideration for I_S will be given below. Thus, the simulation is carried out by generating $I_F(p)$, $I_C(p)$, and I_S, where a certain correlation exists between $I_F(p)$ and $I_C(p)$.

Theoretical Background

Partial Heterodyne Method. The scattering field for polymer gels contains both a fluctuating component and time-independent component since the chain segments between cross-links are allowed a limited Brownian motion within a fixed averaged position.[13] Hence, it may be written by

$$E(t) = E_F(t) + E_C \tag{8}$$

Here the subscripts F and C respectively denote the fluctuating and time-independent properties. The normalized time−intensity correlation function for restricted system can be expressed by[8,41]

$$g_T^{(2)}(q,\tau) \equiv \frac{\langle I(q,t)I(q,t+\tau)\rangle_T}{\langle I(q,t)\rangle_T^2} = 1 + [Xg_F^{(1)}(q,\tau)]^2 + 2X(1-X)g_F^{(1)}(q,\tau) \tag{9}$$

where q is the magnitude of the wave vector, X and $g_F^{(1)}(\tau)$ are the ratio of intensity for the thermal fluctuations to the total intensity and the fully fluctuating component of the field correlation function, respectively. $\langle ... \rangle_T$ denotes time average. That is

$$X \equiv \frac{\langle I_F \rangle_T}{\langle I \rangle_T} \tag{10}$$

$$g_F^{(1)}(\tau) = \frac{\langle E_F(0)E_F^*(\tau)\rangle_E}{\langle I_F(0)\rangle_E} = \frac{\langle E_F(0)E_F^*(\tau)\rangle_T}{\langle I_F(0)\rangle_T} \tag{11}$$

where $\langle ... \rangle_E$ denotes ensemble average. Note that the initial amplitude of the time−intensity correlation function

$$\sigma_I^2 \equiv g_T^{(2)}(0) - 1 = X(2 - X) \tag{12}$$

is less than unity for restricted-ergodic systems due to existence of strong frozen component. As can be found in the collective diffusion theory, $g_F^{(1)}(\tau)$ can be ap-

proximated with a short time expansion as follows

$$g_F^{(1)}(\tau) \cong 1 - Dq^2\tau + ... \quad (13)$$

After trivial mathematical treatment, $g_T^{(2)}(\tau)$ can also be expressed as the following

$$g_T^{(2)}(\tau) = 1 + \sigma_I{}^2(1-2D_Aq^2\tau + ...) \quad (14)$$

where

$$D_A = \frac{X}{\sigma_I{}^2}D \quad (15)$$

From DLS measurements, we obtain D_A, $\sigma_I{}^2$, and $\langle I\rangle_T$ at each sampling point. It is well-known that the correlation function of gels made of acrylamide and its derivatives exhibited almost single-exponential behavior. In the absence of extra slow mode, one can evaluate D_A and $\sigma_I{}^2$ by fitting to eq 14 in the initial decay region, typically in 0.001−0.010 ms. We performed an analysis by systematic data processing with a homemade software for the evaluation of D_A and $\sigma_I{}^2$. First, D_A was determined by the initial slope of the semilogarithmic plot for eq 14, i.e., $\ln[g_T^{(2)}(\tau) - 1]$ vs τ. Subsequently, $\sigma_I{}^2$ was calculated from the extrapolated value to time zero.

Thus, $\langle I_F\rangle_T$ and D can be estimated as a function of sampling position by eq 12 and substitution of eq 12 into eq 15, respectively. We hereafter call the following the single-point partial heterodyne method (SP−PH)[24,42]

$$I_F(p) = I(p)(1 - \sqrt{1 - \sigma_I{}^2(p)}),\ I_C(p) = I(p)\sqrt{1 - \sigma_I{}^2(p)} \quad (16)$$

$$D(p) = D_A(p)[2 - X(p)] = D_A(p)[1 + \sqrt{1 - \sigma_I{}^2(p)}] \quad (17)$$

where we eliminated $\langle ...\rangle_T$ and introduced a symbol p since these parameters can be evaluated in each position. $I_F(p)$ and $D(p)$ will be constant over the sampling positions if there are no dynamic inhomogeneities. On the other hand, if there is certain cross-correlation between static and dynamic components for the scattered intensity, total intensity dependence of $I_F(p)$ and $D(p)$ will positively or negatively deviate from the average for the lower intensity.

Effect of Solvents and/or Sol Fraction. In previous studies, fluctuations have been considered to consist of only two types of fluctuations, namely, the frozen inhomogeneities and the dynamic fluctuations. However, the third component of the scattering field, E_s, due to small molecules such as solvents, sol fraction, and some residues, may be significant for low polymer concentrations or low cross-linking densities. It was first taken into account by Joosten et al.[43] and Rouf et al.,[44] but the effect has been considered to be less important for general cases where the contribution from thermal fluctuations are much larger than that from the third component. In the present study, we will demonstrate the importance of this effect on the position dependent dynamic fluctuations. Adding the third component into the electric fieldyields

$$E(t) = E_F(t) + E_C + E_S(t) \quad (18)$$

Note that the diffusion coefficient for small molecules is on the order of 10^{-5} ($cm^2\ s^{-1}$), which is one order larger than the collective diffusion coefficients in polymer gels. Hence, the decay is hardly observed by a conventional photon correlator, and the correlation function is practically given by

$$\langle I_S(0)I_S(\tau)\rangle = \langle I_S(0)\rangle^2 + |\langle E_S(0)E_S{}^*(\tau)\rangle|^2 \approx \langle I_S(0)\rangle^2 \quad (19)$$

because of

$$\langle E_S(0)E_S{}^*(\tau)\rangle \cong 0 \quad (20)$$

It should be noted that the field correlation is zero but the intensity correlation has nonzero value since the averaged intensity cannot be ignored. With eqs 18−20, we get the following after trivial calculations.

$$g_T^{(2)}(\tau) = 1 + g_F^{(1)}(q,\tau)^2\left(\frac{\langle I_F\rangle_T}{\langle I\rangle_T}\right)^2 + \frac{2I_C\langle I_F\rangle_T}{\langle I\rangle_T{}^2}g_F^{(1)}(q,\tau) \quad (21)$$

$$\sigma_I{}^2\langle I\rangle_T{}^2 = 2\langle I_F\rangle_T\langle I\rangle_T - \{\langle I_F\rangle_T{}^2 + 2\langle I_F\rangle_T\langle I_S\rangle_T\} \quad (22)$$

$$\frac{\langle I\rangle_T - \langle I_S\rangle_T}{D_A} = \frac{2}{D}\langle I\rangle_T - \frac{\langle I_F\rangle_T + 2\langle I_S\rangle_T}{D} \quad (23)$$

By plotting $\sigma_I{}^2\langle I\rangle_T{}^2$ vs $\langle I\rangle_T$, $\langle I_F\rangle_T$ and $\langle I_S\rangle_T$ can be evaluated by the slope and intercept, respectively. Hereafter we call it the modified partial heterodyne method (the modified-PH). On the other hand, D and $\langle I_F\rangle_T$ cannot be obtained independently from eq 23 if $\langle I_S\rangle_T$ is nonzero. However, needless to say, this contribution is negligible for most of the gels (typically less than 1%). It can be concluded that evaluation of $\langle I_F\rangle_T$ and $\langle I_S\rangle_T$ from eq 22 and subsequent estimation of D from eq 23 with fixing $\langle I_F\rangle_T$ and $\langle I_S\rangle_T$ will be a quite acceptable method. By rearrangement of eqs 22 and 23, position-dependent I_F and D will follow (modified SP−PH)

$$I_F(p) = I(p)\left[\left(1 - \frac{I_S}{I(p)}\right) - \sqrt{\left(1 - \frac{I_S}{I(p)}\right)^2 - \sigma_I{}^2(p)}\right] \quad (24)$$

$$D(p) = \frac{D_A(p)[2I(p) - I_F(p) - 2I_S]}{\{I(p) - I_S\}} \quad (25)$$

However, evaluation of $I_F(p)$ and $D(p)$ is not allowed without the information about I_S. Moreover, the estimation of I_S from eqs 22 and 23 may be still difficult in case that the contribution of I_S is much smaller than the dynamic inhomogeneities. Thus, an analysis will be carried out by the SP−PH method using eqs 16 and 17, and then deviation from the results obtained by the SP−PH method will be discussed with the results by the modified PH method.

Results and Discussion

Position-Dependent Intensities and Effect of Small Molecules. As described in the above section, the scattered intensity components for the frozen inhomogeneities, I_C, and the dynamic fluctuations, I_F, can be evaluated in each sampling position by eq 16. The average over a large number of scattering volumes (in this case a hundred points) provides $\langle I_F(p)\rangle_P$, equivalent to that obtained by the partial heterodyne (PH) method as reported before.[24] In Figure 2, the intensity variations are exhibited as a function of sampling position for the PNIPA γ-ray gels with different irradiation dose, i.e., (a, d) 10, (b, e) 50, and (c, f) 80 kGy. Here $I_C(p)$ and $I_F(p)$

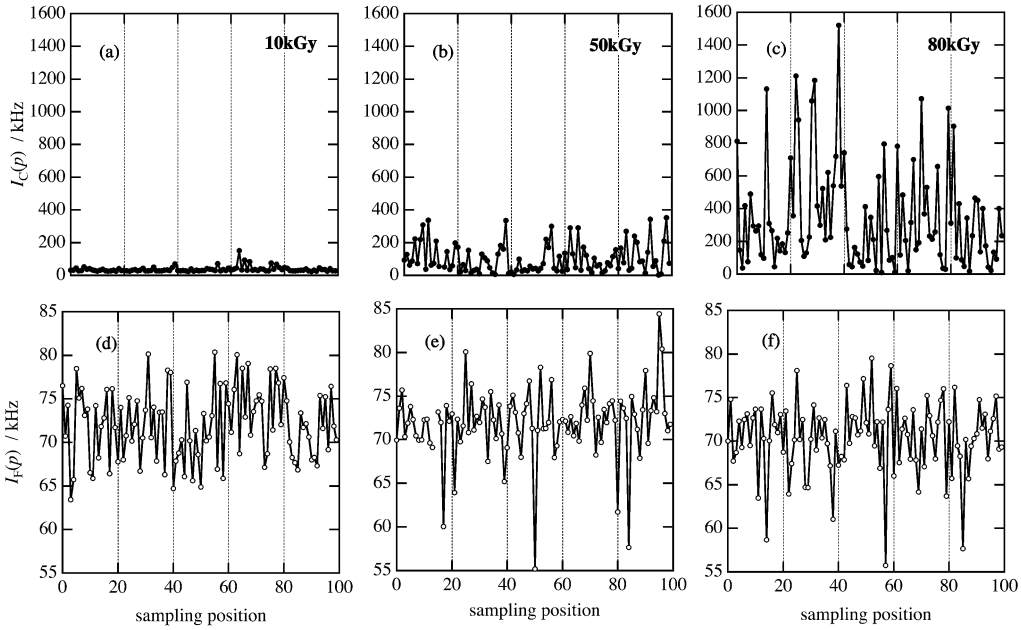

Figure 2. Sampling position dependence of the scattered intensity components for the γ-ray gels with (a, d) 10, (b, e) 50, and (c, f) 80 kGy. Upper and lower parts of the figure correspond to the results for I_C and I_F respectively. Here I_C and I_F respectively denote the intensity components for the frozen inhomogeneities and dynamic fluctuations.

are respectively presented in the upper part (a−c) and the lower part of the figure (d−f). In the previous paper, it is concluded that $I_C(p)$ increases with the irradiation dose whereas $I_F(p)$ remains in rather invariant with the irradiation dose.[28] However, all $I_F(p)$s in the figure seem to fluctuate with position, suggesting the presence of the dynamic inhomogeneities. We would like to stress here these fluctuations include different physical meanings as we will demonstrate latter.

In Figure 3, the ensemble averaged time-field correlation function, $g_E^{(1)}(\tau)$ is exhibited for (a) 10, (b) 50, and (c) 80 kGy. Here the open and closed symbols denote $g_{E,S}^{(1)}(\tau)$ and $g_{E,F-H}^{(1)}(\tau)$, which are derived by Siegert and by Furukawa and Hirotsu,[36] respectively.

$$g_{E,S}^{(1)}(\tau) = \sqrt{g_E^{(2)}(\tau) - 1} = \sqrt{\{\langle\langle I(0)\rangle_T^2 g_T^{(2)}(\tau)\rangle_P\}/\{\langle\langle I(0)\rangle_T^2\rangle_P\} - 1} \quad (26)$$

$$g_{E,F-H}^{(1)}(\tau) = \frac{\langle\langle I(0)\rangle_T \sqrt{g_T^{(2)}(\tau) - \sigma_I^2}\rangle_P}{\langle\langle I(0)\rangle_T\rangle_P} \quad (27)$$

Here, the difference between them is related to the assumption based on eqs 1−3, i.e., spatial coupling being taken into account or not. Furukawa and Hirotsu proposed eq 27, which does not require the estimation of $\delta_E(\tau)$ and is more practical form than eq 1. As seen from the figure, all the correlation functions feature a nonzero baseline, a characteristic in gelling systems due to the frozen component. However, $g_{E,S}^{(1)}(\infty)$ is always smaller than $g_{E,F-H}^{(1)}(\infty)$, suggesting the existence of a certain correlation between E_F and E_C. Although the physical meaning of $\delta_E(\tau)$ in eq 1 is not provided in the literature, one should be aware that the effect of $\delta_E(\tau)$ may lead to serious misleading of the dynamics and the corresponding intensity when the effect of the spatial coupling is ignored. As shown in the inset of the figure, plots of $\sigma_I^2 I^2$ vs I give good straight lines for all samples, allowing us to evaluate $\langle I_F\rangle_P$ and $\langle I_C\rangle_P$ as well as $\langle I_S\rangle_T$. The baseline represented by solid lines is reproduced by the partial heterodyne method, $g_{E,PHD}^{(1)}(\infty)$, with

$$g_{E,PHD}^{(1)}(\infty) = \frac{\langle I_C\rangle_P}{\langle I_F\rangle_T + \langle I_C\rangle_P + \langle I_S\rangle_T} \quad (28)$$

which is represented by solid lines. The results seem to be rather close to the value for $g_{E,F-H}^{(1)}(\infty)$ except that for 10 kGy. For 50 and 80 kGy, it is natural since the partial heterodyne method dose not assume independence of I_C and I_F but is based on the time-averaged quantities. Note that $g_{E,PHD}^{(1)}(\infty)$ significantly differs from $g_{E,F-H}^{(1)}(\infty)$ for 10 kGy. This is due to $\langle I_S\rangle_T$, which is not taken into account in the F−H equation. The difference will be more serious when position dependent dynamic fluctuations become nontrivial.

Let us demonstrate simple simulations in advance to accurate analysis of the dynamic inhomogeneities. First 100 points of $I_F(p)$ and $I_C(p)$ were generated by eqs 5 and 6 with a certain correlation between them. In addition to the position dependence of $I_F(p)$ and $I_C(p)$, a constant value of I_S is also considered here to generalize our discussion. Subsequently, $\sigma_I^2(p)$ is calculated by eq 22 with $\langle I_F\rangle_P/\langle I\rangle_P = 0.10$ and $I_S/\langle I\rangle_P = 0.02$. Then $\sigma_I^2(p)$ was sorted by the total intensity $I(p)$ together with the intensity components, followed by reconstruction of $I_F(p)$ by the conventional equation of eq 16. Figure 4 exhibited simulated curves where the negative or positive correlation exists between $I_F(p)$ and $I_C(p)$. The solid and dotted lines indicate respectively the intensity variation of $I_F(p)$ in the absence (curves A, C, and E) and presence (B, D, and F) of I_S with $I_S/\langle I\rangle_P = 0.02$. For the positive correlation system (A, B), $I_F(p)$ increased with the total intensity, $I(p)$, whereas $I_F(p)$ decreased with $I(p)$ for the negative correlation system (E, F). Needless to say, it remains in a constant in the absence of both the spatial correlation and I_S (C). It should be noted that the increasing of $I_F(p)$ with $I(p)$ is also observable for $I_S/\langle I\rangle_P = 0.02$ without any correlation because of the considerable contribution of I_S for the

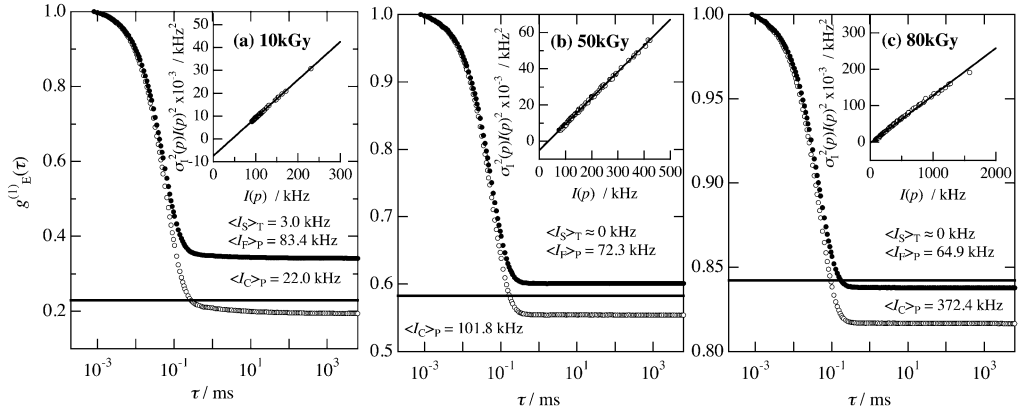

Figure 3. Ensemble averaged time-field correlation functions for the γ-ray gels with (a) 10, (b) 50, and (c) 80 kGy. Open and closed symbol denote $g_E^{(1)}(\tau)$ calculated with eqs 26 and 27, respectively. The inset of the figure indicates the results of modified partial heterodyne (modified-PH) method with a hundred sets of $I(p)$ and $\sigma_I^2(p)$. $g_E^{(1)}(\infty)$ is also predicted by the results as indicated by the solid lines.

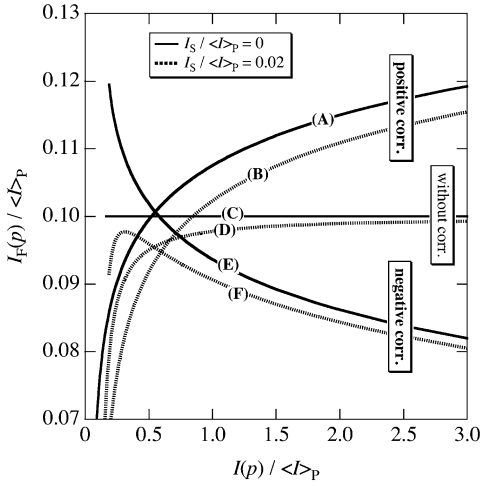

Figure 4. Simulated curves for $I_F(p)/\langle I\rangle_P$ with $\langle I_F\rangle_P/\langle I\rangle_P = 0.10$, where the increasing and decreasing curves respectively indicate the data with positive (curves A and B) and negative (E and F) correlations between $I_F(p)$ and $I_C(p)$. Curves (C) and (D) indicate $I_F(p)/\langle I\rangle_P$ without the correlation. The solid lines and dashed lines indicate respectively the data with $I_S/\langle I\rangle_P = 0$ and $I_S/\langle I\rangle_P = 0.02$.

lower intensity (D; see eq 24). Moreover, if a negative correlation exists between $I_F(p)$ and $I_C(p)$ with $I_S/\langle I\rangle_P = 0.02$, the variation of $I_F(p)$ will be characterized by a curve with a maximum (F).

Next, we present the experimental results for the PNIPA γ-ray gels analyzed by eq 16. $I_F(p)$ should be a constant over the various intensities provided that no spatial correlation and no additional scatters are present. However, $I_F(p)$s significantly deviated from the average for the lower intensity as shown in Figure 5. Here $I_C(p)$ is also exhibited in the right axis. For 10 and 80 kGy, the obtained data show an opposite tendency, i.e., a downward and upward function with $I(p)$, respectively. The contribution from $I_S = 3.0$ kHz was evident according to the above analysis for 10 kGy. (Figure 3a) Therefore, it can be concluded that the position dependent fluctuations in $I_F(p)$ for 10 kGy (Figure 2d) includes the indispensable contributions from I_S, which is unconsidered in eq 16. On the other hand, there is no noticeable contribution from I_S for 80 kGy (Figure 3f) and $I_F(p)$ shows rather opposite tendency compared to that for 10 kGy. An interpretation with another possible component is not allowed in this case because it leads

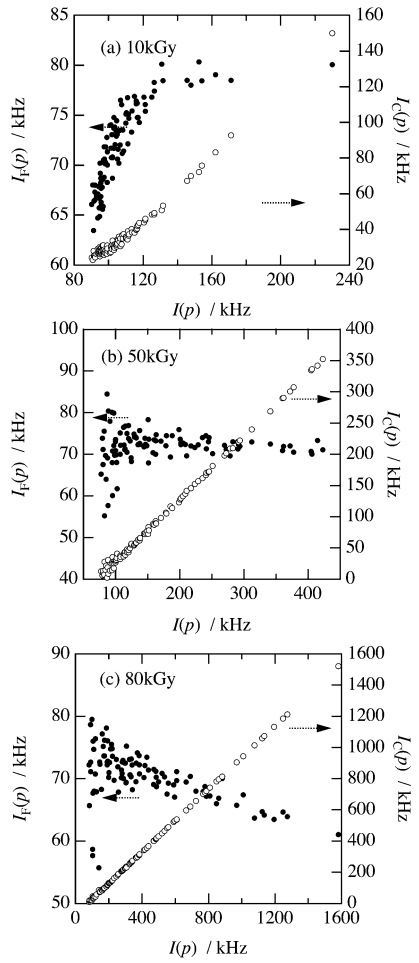

Figure 5. Total intensity dependence for $I_F(p)$ and $I_C(p)$ for (a) 10, (b) 50, and (c) 80 kGy. As seen from the figure, the significant reduction of $I_F(p)$ was found for 10 kGy, whereas opposite behavior to 10 kGy was found for 80 kGy. For 50 kGy, intermediate behavior between parts a and c was observed.

to a rather negative intensity value, resulting in unphysical outcome. According to the classical theory, the scattered intensity component for the thermal fluctuations may be written as

$$I_F(q) = \Delta\rho^2 \frac{k_B T \phi^2}{M_{os}} \frac{1}{1 + q^2\xi^2} \qquad (29)$$

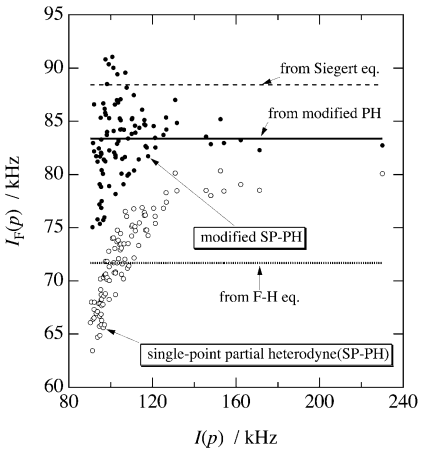

Figure 6. $I_F(p)$ results for 10 kGy by the single point partial heterodyne (SP−PH; eq 16) method and that with the extra component correction (the modified SP−PH; eq 24) are denoted by open and closed symbols. Here $\langle I_F\rangle_P$ obtained by the Siegert equation (eq 26), the Furukawa−Hirotsu equation (eq 27), the and modified-PH (eq 28) are presented by dashed line, dotted line, and solid line, respectively.

where $\Delta\rho^2$, k_BT, ϕ, M_{OS}, ξ are the scattering contrast, the Boltzmann energy, the volume fraction of polymer, the longitudinal osmotic modulus, and the thermal correlation length, respectively. For polymer gels, M_{OS} is given by[41]

$$M_{OS} = \phi\frac{\partial\omega}{\partial\phi} + \frac{4}{3}G \tag{30}$$

where ω and G are the swelling pressure of the network and the shear modulus, respectively. The reduction of $I_F(q)$ can be easily understood from eqs 29 and 30 as increasing the cross-linking density. On the other hand, increasing of $I(p)$ as well as I_C may be attributed to increasing of the local cross-linking density. Thus, we concluded that the negative correlation between I_F and I_C is a signature of the dynamic inhomogeneities, which emerges owing to the different molecular environments, such as the gel concentration and the cross-linking density as illustrated in Figure 1.

To demonstrate the effect of small molecules on the data analysis, $I_F(p)$ obtained by the single-point partial heterodyne equation (SP−PH; eq16) and that with I_S correction (modified-SP−PH; eq24) is compared. In Figure 6, $I_F(p)$ for 10 kGy was presented as a function of $I(p)$, where open and closed symbols denote the results with the SP−PH and the modified-SP−PH, respectively. Compared with the open symbols, decreasing of $I_F(p)$ in the low $I(p)$ region disappeared for the closed symbols, resulting in similar intensity dependence with that for 50 kGy (Figure 5b). Here $\langle I_F\rangle_P$s calculated by the Siegert equation (eq 26), the Furukawa−Hirotsu equation (F−H, eq 27), and the modified partial heterodyne equation (modified-PH, eq 22) are indicated together by the dashed line, the dotted line, and the solid line, respectively. As seen from the figure, the Siegert equation obviously overestimated $\langle I_F\rangle_P$. On the other hand, the F−H equation seems to produce an average value of $I_F(p)$ obtained by SP−PH without the correction of I_S. This result is reasonable because neither the Siegert equation nor the F−H equation takes account of the contribution from I_S. Note that noticeable contribution from I_S was not found for a higher irradiation dose. For gels with higher irradiation dose, all the methods except for the Siegert equation provide almost the same result.

Diffusion Coefficient. If there exist dynamic inhomogeneities in polymer gels, a characteristic behavior should appear not only in the scattered intensity but also in the diffusion coefficient. In Figure 7, the variation of diffusion coefficients with the total intensity, $I(p)$, are exhibited for (a) 10, (b) 50, and (c) 80 kGy, where open circles and squared symbols denote the apparent diffusion coefficient, $D_A(p)$, and the homodyne diffusion coefficient, $D(p)$, calculated by eq 25, respectively. The diffusion coefficient, D, evaluated by the extrapolation of $D_A(p)$ to the homodyne limit with eqs 22 and 23, is exhibited by the dotted line. Since the effect of the frozen inhomogeneities is taken into account, $D(p)$ should be a constant value of D over various $I(p)$s. Nevertheless, $D(p)$ for 10 kGy exhibited a significant upturn at the lower $I(p)$. This is again due to the effect of I_S not only on $I_F(p)$ but also on the initial decay rate of the correlation functions as well as D_A (eq 14). Therefore, $D(p)$ was further corrected by

$$D_{corr} = D\frac{I_F(p)}{I_{F,corr}(p)} \tag{31}$$

where $I_F(p)$ and $I_{F,corr}(p)$ respectively were calculated by eqs 16 and 24. After the correction, D_{corr} became fairly constant as indicated by the solid square in Figure 7a. For 50 kGy in Figure 7b, $D(p)$ seems to be rather constant over various $I(p)$s without I_S correction. Finally, $D(p)$ for the highest irradiation dose, 80 kGy, where the dynamic inhomogeneities were found, is exhibited in Figure 7c. As indicated by the solid curve, reduction of $D(p)$ in the lower $I(p)$ region was followed by gradual increasing of $D(p)$. Since there is an inverse relation between $I_F(p)$ and $D(p)$, the variation of $D(p)$ is consistent with the finding stated above (see Figure 5c). However, the present data are not enough to prove the presence of an I_S contribution. Hence we envisaged that the effect of the dynamic inhomogeneities might be explicit by eliminating the contributions from sol fraction and/or residues.

The variation of the diffusion coefficient was compared between the as-prepared gels and the washed gels. Figure 8 exhibits the normalized diffusion coefficient, $D(p)/D$, as a function of the normalized intensity, $I(p)/\langle I\rangle_P$, for the γ-ray gels with an irradiation dose of 50 kGy where D is the homodyne diffusion coefficient evaluated by the modified PH method. As seen from the figure, reduction of $D(p)/D$ in the lower intensity part becomes explicit for the washed gels. Thus, it is concluded that the speculation of the above finding in Figure 7c is reasonable. Namely, (1) the total intensity dependence of $D(p)$ exhibits antagonistic behavior compared to $I_F(p)$ where the variation due to the dynamic inhomogeneities can be clearly seen, and (2) the effect of I_S is significant for low $I(p)$ in order to evaluate $I_F(p)$ as well as $D(p)$, resulting in suppression of the specific reduction of $D(p)$. Note that D for the as-prepared and the washed gels are almost the same, i.e., 4.67×10^{-7} and 4.76×10^{-7} cm^2 s^{-1}, suggesting that the effect of the structural reconstruction by washing is not a major reason for the difference of $D(p)/D$.

In Figure 9, $D(p)/D$ vs $I_F(p)/\langle I_F\rangle_P$ for the PNIPA-SA with various pHs are demonstrated. The linear swelling ratio, d/d_0, is also presented in the legend. For low pHs, e.g., pH = 3, dissociation of proton is not promoted,

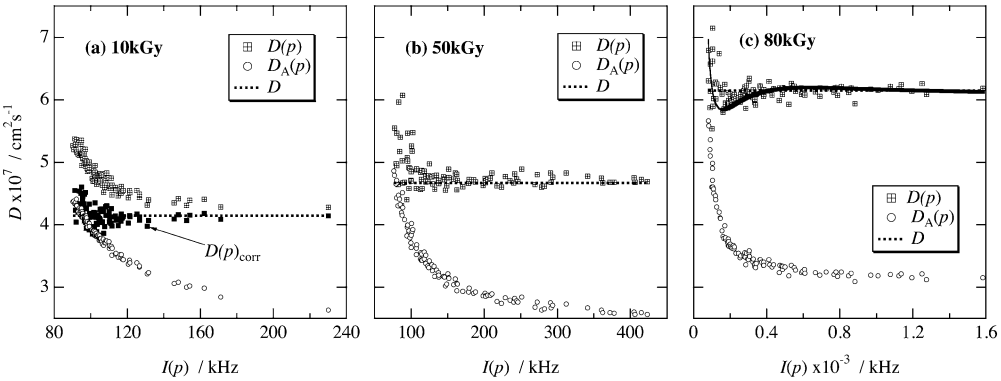

Figure 7. Apparent diffusion coefficient, D_A, evaluated by eq 14, the homodyne diffusion coefficient, D, evaluated by eq 17 and the predicted line obtained by modified-PH are represented by open symbols, squared symbols and solid line, respectively, for the γ-ray gels with (a) 10, (b) 50, and (c) 80 kGy. For 10 kGy, $D(p)$ was further corrected by $I_F(p)/I_{F,corr}(p)$. For 80 kGy, the reduction of $D(p)$ for the lower $I(p)$ is expected as indicated by the solid line.

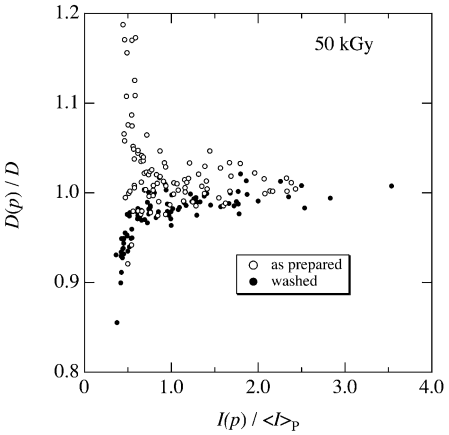

Figure 8. Normalized diffusion coefficient, $D(p)/D$, as a function of the normalized intensity, $I(p)/\langle I\rangle_P$, for the γ-ray gels with the irradiation dose of 50 kGy where D is the homodyne diffusion coefficient evaluated by the modified-PH method. Open and closed symbols represent respectively the results for the as-prepared gels and the washed gels.

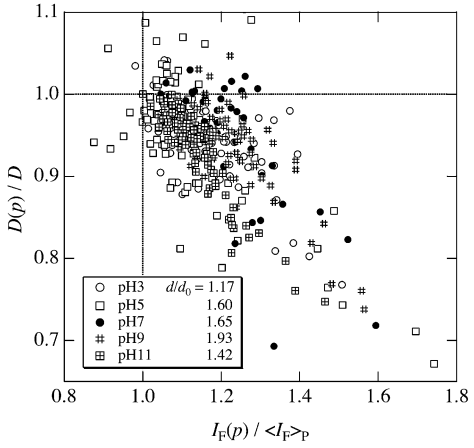

Figure 9. $D(p)/D$ vs $I_F(p)/\langle I_F\rangle_P$ plot for the PNIPA-SA gels with various pHs. The values of $D(p)/D$ are heavily overlapped independent of pH as well as of linear swelling ratio, d/d_0.

resulting in a similar d/d_0 with the PNIPA gels without SA. With increasing pH, the gel swells due to osmotic pressure generated by counterions of ionized SA groups. For pH = 9, a maximum swelling ratio is attained. Further increasing of pH leads to decreasing of d/d_0 due to screening of the electrostatic interaction. Here the pH dependence for $D(p)/D$ was investigated in order to make sure whether the dynamic inhomogeneities be-

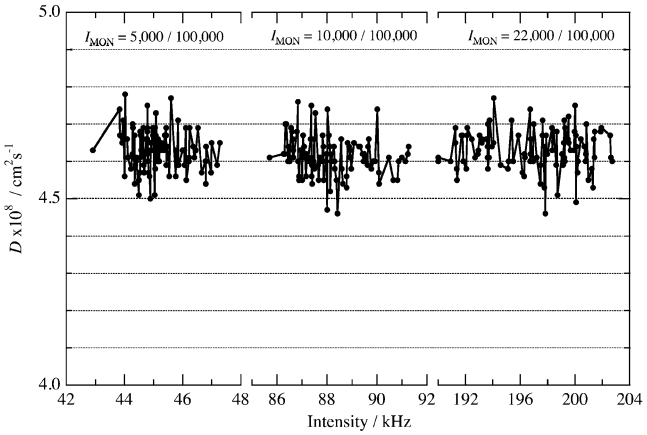

Figure 10. Scattered intensity dependence of the diffusion coefficient D for the standard latex with the diameter of 85 nm. The measurements were carried out in order to demonstrate the accuracy of D against the incident beam power as well as the rotation of the test tube.

come larger with the swelling or not. As shown in the figure, the values of $D(p)/D$ are scattered below unity for all the pHs studies here. However, as seen from the figure, the variation of $D(p)/D$ with $I_F(p)/\langle I_F\rangle_P$ indicated almost the same values independent of pH. Hence, it can be concluded that dynamic inhomogeneities exist in polymer gels regardless of the swelling degree. It should be noted, however, the magnitude of the dynamic inhomogeneities seems to be invariant after normalization with respect to the degree of swelling.

So far, we have been demonstrating the position dependent dynamic fluctuations obtained by DLS. However, one may criticize that such kind of behavior is due to artifact such as, glass cell inhomogeneities and/or stability of the detection against rotation. To make sure this point, DLS measurements for the standard latex solutions (diameter of 85 nm, $c = 0.001\%$) were carried out at more than a hundred sampling points. A series of measurements are also performed at different incident beam power in order to check the effects of low counting rate and the neutral density filter. The results are summarized in Figure 10. The diffusion coefficients are located around $D = (4.64 \pm 0.16) \times 10^{-8}$ cm^2 s^{-1} for all the beam powers. As seen from the figure, the values of D are fairly constant, and no tendency to vary upward or downward within a hundred sampling positions. Furthermore, D is also invariant with respect to the monitor intensity, leading to successful validation of the position dependent dynamic fluctuations.

Two remarks should be noted before the conclusion. (1) $I_F(p)$ is *not directly* related to the local structure at the position p. Since the scattering properties are observed as a result of interference of scattering field originated from two different positions apart from $1/q$ and are summed up in the scattering volume, the scattering properties are strongly dependent not only on the scattering volume determined by the position, p, but also on the range given by $1/q$ around the position, p. These values, however, *still contain* information about the local structure around the position, p, as non-canceled-out correlation of concentration fluctuations. Hence, the observed quantities, such as $I_F(p)$ and $I(p)$ carry information on the inhomogeneities of gel structure. (2) Elucidation of the existence and kind of correlation between $I_F(p)$ and $I(p)$ was one of the main issues of this paper. It was revealed here that any additional scatterings other than those originating from gels result in positive correlation between $I_F(p)$ and $I(p)$ as proved in Figures 6 and 7. The positive correlation strongly indicates a significant contribution of the solvent scattering. On the other hand, a negative correlation is a logical conclusion reflecting the physical pictures of gel structure. This fact was clearly detected by this analysis.

Conclusions

Static and dynamic inhomogeneities of polymer gels have been investigated by dynamic light scattering (DLS). We demonstrated the position dependent intensities for the frozen and dynamic components, denoted respectively by $I_C(p)$ and $I_F(p)$, for various types of gels, where $I_C(p)$ and $I_F(p)$, were evaluated from the intensity decomposition analysis, called the single point partial heterodyne (SP−PH) method. The following five major findings were drawn. (1) Although all the gels investigated in this study exhibited more or less the presence of position dependence in both $I_C(p)$ and $I_F(p)$, it was found that $I_F(p)$ with the lowest cross-linking density, e.g., the γ-ray gels with the irradiation dose of 10 kGy, exhibited effects of an extra scattering component in addition to the dynamic inhomogeneities. (2) In contrast, the dynamic inhomogeneities became obvious with increasing the cross-linking density. It can be resolved by sorting the $I_F(p)$ with $I(p)$ or $I_C(p)$ with an aid of the cross-correlation between $I_F(p)$ and $I_C(p)$. (3) It was concluded that the negative correlation between $I_F(p)$ and $I_C(p)$ was attributed to a consequence of the dynamic inhomogeneities. The dynamic inhomogeneities were physically interpreted as the difference of the molecular environments, such as the local cross-linking density and segmental concentration. The results for the homodyne diffusion coefficient also supported these findings. The theory was further developed in order to account for opposite intensity dependence of $I_F(p)$. (4) In this study, a third component, I_S, the sol faction and some residues, was also taken into account in addition to I_F and I_C. Although I_S is weak compared to I_F and I_C, it imposes a serious reduction of I_F for the case with the low total intensity. The significance of the effect of I_S was confirmed by a comparison between as-prepared gels and washed gels. Needless to say, it affects the evaluation of the dynamic inhomogeneities. (5) Contrary to the total intensity dependence of $I_F(p)$ and $D(p)$, the magnitude of the dynamic inhomogeneities is rather invariant of swelling degree. This means that the dynamics are highly restricted by cross-links around its average, which will be dominated by the number of cross-links in a gel.

Acknowledgment. This work is supported by Grants-in-Aid, Nos. 12450388, 13750832, and 14350493 and Grants-in-Aid for Scientific Research on Priority Areas (A), "Dynamic Control of Strongly Correlated Soft Materials" (No. 413/13031019 and No. 413/14045216) from the Ministry of Education, Science, Sports, Culture, and Technology.

References and Notes

(1) Rossi, D.; Kajiwara, K.; Osada, Y.; Yamauchi, A., Eds. *Polymer Gels*; Plenum: New York, 1991.
(2) Osada, Y.; Kajiwara, K., Eds. *Gel Handbook*; Academic Press: New York, 2001.
(3) Bastide, J.; Leibler, L. *Macromolecules* **1988**, *21*, 2647.
(4) Bastide, J.; Candau, S. J. In *The Physical Properties of Polymer Gels*; Cohen Addad, J. P., Ed.; John Wiley: New York, 1996; Vol. Chapter 9, p 143.
(5) Mallam, S.; Horkay, F.; Hecht, A. M.; Geissler, E. *Macromolecules* **1989**, *22*, 3356.
(6) Hecht, A. M.; Horkay, F.; Mallam, S.; Geissler, E. *Macromolecules* **1992**, *25*, 6915.
(7) Mendes, E.; Girard, B.; Picot, C.; Buzier, M.; Boue, F.; Bastide, J. *Macromolecules* **1993**, *26*, 6873.
(8) Joosten, J. G. H.; McCarthy, J. L.; Pusey, P. N. *Macromolecules* **1991**, *24*, 6690.
(9) Xue, J. Z.; Pine, D. J.; Milner, S. T.; Wu, X. L.; Chaikin, P. M. *Phys. Rev. A* **1992**, *46*, 6550.
(10) Shibayama, M.; Takeuchi, T.; Nomura, S. *Macromolecules* **1994**, *27*, 5350.
(11) Rodd, A. B.; Dunstan, D. E.; Boger, D. V.; Schmidt, J.; Burchard, W. *Macromolecules* **2001**, *34*, 3339−3352.
(12) Zhao, Y.; Zhang, G.; Wu, C. *Macromolecules* **2001**, *34*, 7404.
(13) Pusey, P. N.; van Megen, W. *Physica A* **1989**, *157*, 705.
(14) Pusey, P. N. *Macromol. Symp.* **1994**, *79*, 17.
(15) Rouf-George, C.; Munch, J.-P.; Schosseler, F.; Pouchelon, A.; Beinert, G.; Boue, F.; Bastide, J. *Macromolecules* **1997**, *30*, 8344.
(16) Shibayama, M.; Shirotani, Y.; Shiwa, Y. *J. Chem. Phys.* **2000**, *112*, 442.
(17) Motonaga, T.; Shibayama, M. *Polymer* **2001**, *42*, 8925.
(18) Bastide, J.; Boue, F.; Buzier, M. In *Molecular Basis of Polymer Networks*; Baumgartner, A., Picot, C. E., Eds.; Springer-Verlag: Berlin, 1989; p 48.
(19) Bastide, J.; Leibler, L.; Prost, J. *Macromolecules* **1990**, *23*, 1821.
(20) Mendes, E. J.; Lindner, P.; Buzier, M.; Boue, F.; Bastide, J. *Phys. Rev. Lett.* **1991**, *66*, 1595.
(21) Rouf, C.; Bastide, J.; Pujol, J. M.; Schosseler, F.; Munch, J. P. *Phys. Rev. Lett.* **1994**, *73*, 830.
(22) Shibayama, M.; Kawakubo, K.; Ikkai, F.; Imai, M. *Macromolecules* **1998**, *31*, 2586.
(23) Rabin, Y.; Panyukov, S. *Macromolecules* **1997**, *30*, 301.
(24) Shibayama, M.; Norisuye, T.; Nomura, S. *Macromolecules* **1996**, *29*, 8746.
(25) Sato-Matsuo, E.; Orkisz, M.; Sun, S.-T.; Li, Y.; Tanaka, T. *Macromolecules* **1994**, *27*, 6791.
(26) Shibayama, M.; Takata, S.; Norisuye, T. *Physica A* **1998**, *249*, 245.
(27) Norisuye, T.; Masui, N.; Kida, Y.; Shibayama, M.; Ikuta, D.; Kokufuta, E.; Ito, S.; Panyukov, S. *Polymer* **2002**, *43*, 5289−5297.
(28) Norisuye, T.; Kida, Y.; Masui, N.; Tran-Cong-Miyata, Q.; Maekawa, Y.; Yoshida, M.; Shibayama, M. *Macromolecules* **2003**, *36*, 6202.
(29) Shibayama, M.; Fujikawa, Y.; Nomura, S. *Macromolecules* **1996**, *29*, 6535.
(30) Takata, S.; Norisuye, T.; Shibayama, M. *Macromolecules* **2002**, *35*, 4779.
(31) Norisuye, T.; Shibayama, M.; Nomura, S. *Polymer* **1998**, *39*, 2769.
(32) Norisuye, T.; Shibayama, M.; Tamaki, R.; Chujo, Y. *Macromolecules* **1999**, *32*, 1528.
(33) Norisuye, T.; Inoue, M.; Shibayama, M.; Tamaki, R.; Chujo, Y. *Macromolecules* **2000**, *33*, 500.

(34) Takata, S.; Norisuye, T.; Tanaka, N.; Shibayama, M. *Macromolecules* **2000**, *33*, 5470.
(35) Geissler, E.; Horkay, F.; Hecht, A.-M. *Macromolecules* **1991**, *24*, 6006.
(36) Furukawa, H.; Hirotsu, S. *J. Phys. Soc. Jpn.* **2002**, *71*, 2873.
(37) Siegert, A. F. J. *MIT Radiat. Rep.* **1943**, *465*.
(38) Naghash, H. J.; Okay, O. *J. Appl. Polym. Sci.* **1996**, *60*, 971.
(39) Patras, G.; Qiao, G. G.; Solomon, D. H. *Macromolecules* **2001**, *34*, 6369.
(40) Ide, N.; Fukuda, T. *Macromolecules* **1999**, *32*, 95.
(41) Geissler, E. In *Dynamic Light Scattering, the Methods and Applications*; Brown, W., Ed.; Oxford University: Oxford, England, 1993.
(42) Fang, L.; Brown, W. *Macromolecules* **1992**, *25*, 6897.
(43) Joosten, J. G. H.; Gelade, E. T. F.; Pusey, P. N. *Phys. Rev. A* **1990**, *42*, 2161.
(44) Rouf-George, C.; Munch, J. P.; Schosseler, F.; Pouchelon, A.; Beinert, G.; Boué, F.; Bastide, J. *Macromolecules* **1997**, *30*, 8344.

MA035246D